2020 8th IEEE International Conference on Biomedical
Robotics and Biomechatronics (BioRob)
New York, USA. Nov 29 - Dec 1, 2020

Muscle-level analysis of trunk mechanics via musculoskeletal modeling and high-density electromyograms

Alejandro Moya-Esteban[1], Niels P. Brouwer[2], Ali Tabasi[2], Herman van der Kooij[1], Idsart Kingma[2] and Massimo Sartori[1]

Abstract— **Back-support (BS) exoskeletons aim at preventing or minimizing low-back pain in workers within occupational environments. Currently, there is no consensus on the optimal controller for BS exoskeletons. We propose a controller based on electromyography (EMG)-informed musculoskeletal modeling that estimates back muscle-tendon forces and moments. In this study, we validate an EMG-driven trunk model to estimate flexion-extension moments at the lumbar L5/S1 joint, during symmetric lifting tasks. In a first experimental session, ground reaction forces, subject kinematics and bipolar EMG activity from abdominal and lumbar muscles were recorded to estimate L5/S1 moments using both, inverse dynamics (ID) and EMG-driven modeling approaches. One subject performed squatting and stooping lifting tasks with three weight conditions (0, 5 and 15 kg). Correlation coefficients, R^2, between reference moments (from ID) and corresponding EMG-driven estimates ranged between 0.94 and 0.98, with root mean squared errors between 10.23 and 20.30 Nm. In a second experimental session, 4 high-density EMG (HDEMG) grids (256 channels) were used to generate high-fidelity topographical activation maps of thoracolumbar muscles during lifting tasks. These maps revealed that lifting objects using the squatting technique, underlay a shift of activation from caudal muscle trunk regions to cranial areas while lowering the weights. Muscle forces derived from EMG-driven modeling altogether with HDEMG activation maps are here proposed as a new framework to understand trunk neuromechanics during complex lifting tasks.**

I. INTRODUCTION

Physically demanding tasks such as heavy object lifting or prolonged stooped postures have a high prevalence within occupational environments. These activities take a toll on the human musculoskeletal system. As a result, low back and shoulder pain are present in more than 40% of the European working population [1]. Physical loading of the low back has been regarded as one of the main contributors to the development of chronic low back pain (LBP) [2]. LBP does not only have an impact on workers' quality of life, but it also entails an economical burden due to the costs related to diagnosis and treatment.

Robotic exoskeletons have the capacity to enhance human motor capabilities. These devices augment human power by providing assistive forces or torques to a single or multiple joints. In a clinical setting, patients suffering from neuromusuclar disorders or disabilities, such as spinal cord injury or post-stroke patients, can see their motor function improved or even restored by using this technology [3]. Exoskeletons have also been developed to increase muscular strength and endurance in military tasks, such as carrying heavy objects [4]. However, applications are not limited to clinical or military settings. In the past years, much focus has been placed on occupational scenarios [5].

Back-support exoskeletons (i.e. trunk exoskeletons), are designed to relieve back musculature and spine loading. Therefore, they could play a key role in preventing LBP. Their potential relies on their ability to provide assistive torques while maintaining the freedom and flexibility of human movements. Compared to passive models, active back-support exoskeletons are generally able to provide greater assistance levels in a much more controlled manner. They provide assistive torques generated by electric motors, hydraulic or pneumatic actuators and the onset of actuation and its magnitude are dictated by a controller. Hence, physical loading on workers spine and musculature may be reduced, which may decrease the incidence of work-related injuries.

Currently, there is no consensus on the best strategy to control back-support exoskeletons for preventing LBP. Some controllers rely on physiological or biomechanical variables, which can be measured using non-invasive techniques. For instance, some controllers aim at minimizing electromyographic (EMG) activity of back muscles [6]. However, given the highly non-linear relation between EMG and joint loading, a reduction in back muscles EMG does not necessarily involve a reduction in spine loading. On the contrary, individual back muscle forces directly relate to the magnitude of compressive forces exerted on intervertebral joints. Previous biomechanical studies suggest that the lumbo-sacral joint (L5/S1) exhibits peak compressive forces in a variety of tasks, such as object lifting and lowering. Such peak compressive forces can rise as high as 5000 N lifting a weight of 15 kg [7]. However, to the best of our knowledge, there is no controller considering estimates of back muscle forces and spine compressive forces in their control action.

Another factor to take into account in the design of back-support exoskeleton controllers is the neuromechanics of thoracolumbar muscles. Many studies have examined the spatial distribution of muscle activation across lumbar, thoracic and cervical muscles in both, healthy and LBP patients, during fatiguing and non-fatiguing tasks [8]. However, there is no full understanding of such EMG activation strategies and how they result in mechanical forces. In the past years, high-density surface EMG (HDEMG) has provided new

*This work is part of the research program Wearable Robotics, project number P16-05, (partly) financed by the Dutch Research Council (NWO).

[1]Department of Biomechanical Engineering, University of Twente, Enschede, The Netherlands

[2]Department of Human Movement Sciences, Faculty of Behavioural and Movement Sciences, Vrije Universiteit Amsterdam, Amsterdam, The Netherlands

perspectives on the field due to its potential to measure the EMG distribution over large surface areas, such as that spanned by the erector spinae muscle.

Our ultimate goal is to implement exoskeleton controllers, whose assistance will maintain spinal compressive forces within acceptable limits. Before implementing such controllers, it is necessary to understand trunk muscle recruitment strategies and how active muscles contribute to generate forces, in a large repertoire of tasks. Most state of the art approaches focus on inverse dynamics (ID) analyses of spinal joint mechanics, and on low density EMG measurements. However, these studies cannot provide a full understanding of trunk neuromechanics because trunk muscles span large areas so low-density EMG recordings cannot capture whole-muscle activation patterns [8], and ID analyses do not provide any insight on force generation patterns at a muscle level [9]. The main goal of the present study is to provide, for the first time, a framework based on modeling and HDEMG for deriving high-resolution estimates of trunk muscle activity and resulting muscle-tendon forces and joint moments, during a large range of box lifting conditions.

II. METHODS

A. Subjects and apparatus

One male subject (26 years old; body mass: 68.0 kg; height: 1.75 m) participated in the experiment. The participant did not have any history of LBP in the past.

Ground reaction forces (GRF) and moments were measured using an AMTI dual force plate (AMTI, MA, USA). In both experimental sessions, the subject placed one foot on each individual plate and signals were recorded at 2048 Hz.

Qualisys motion capture system (Qualisys Medical AB, Gothenburg, Sweden) was used to measure subject full-body and box kinematics. Ten infrarred Oqus cameras recorded the 3D trajectories of 70 spherical reflective markers (62 on the subject and 1 on each corner of the box). Marker position was recorded at 128 Hz. In order to linearly scale the anthropometry of the generic musculoskeletal model, 22 out of the 62 markers were were placed on (right and left): medial and lateral malleoli, medial and lateral femur epicondyles, great trochanters, medial and lateral humeral epicondyles, ulnar and radial styloids and 2^{nd} and 5^{th} knuckles. Cluster markers (triplets) were used to track subject kinematics during inverse kinematics (IK) computation. A total of 24 cluster markers were used to track 8 body segments (right and left): shanks, thighs, upper arms and forearms. Other markers were used for both, scaling and IK: right acromions, sternum, C7, T10, anterior and posterior iliac spines, 1^{st} and 5^{th} metatarsus and calcaneus.

In experimental session I (see section II-C.1), EMG activity from lumbar and abdominal muscles was measured with the Delsys Bagnoli system (Delsys Bagnoli, Delsys, Boston, MA) at 2048 Hz. 12 EMG bipolar electrodes were placed bilaterally on the subject following previously described guidelines [10]. Ventrally, we measured the activity of the rectus abdominis muscle (umbilicus level), the internal oblique muscle (superior to the inguinal ligament), and the lateral part of the external oblique muscle (midaxillary line, halfway between the iliac crest and the lowest edge of the rib cage). Dorsally, electrodes were attached over the iliocostalis lumborum muscle (6 cm lateral to L2) and over the longissimus thoracis pars lumborum (3 cm lateral to L1) and pars thoracis (4 cm lateral to T10).

In experimental session II (see section II-C.2), HDEMG activity was measured with the Refa system (TMSi, Oldenzaal, The Netherlands) and 4 semidisposable 8×8 grids. Each grid comprised 64 electrodes evenly spaced (inter-electrode distance of 8.5 mm) and had surface of 71×76 mm. The electrodes were adhered to the skin unilaterally, 1 cm right to the spine. The bottom grid was placed immediately above the posterior iliac spine, at the level of L5. The rest of the grids were stacked one on top of another, with an inter-grid distance of 3-5 mm. Given the height of the subject, the top border of the uppermost grid was located at the height of the inferior angle of the scapula.

Marker position, GRF, bipolar and HDEMG signals were synchronized by Qualisys Track Manager software.

B. EMG-driven musculoskeletal modeling

A framework based on our previously proposed calibrated EMG-informed neuromusculoskeletal modeling toolbox (CEINMS) [11], [12] was used to estimate net L5/S1 joint moments and musculotendon unit (MTU) forces based on joint angles and EMG recordings. Fig. 1 depicts a block diagram of the model and its main components.

A previously validated musculoskeletal model [9] was also used to calculate L5/S1 joint moments. The model, known as lifting full-body model (LFB), comprises 30 segments, 29 degrees of freedom and 238 Hill-type MTU representing trunk muscles. This model was used to obtain joint angles (via IK) and joint torques (via ID). IK-derived joint angles were used as input by CEINMS and ID-derived joint torques were used in the calibration stage of CEINMS.

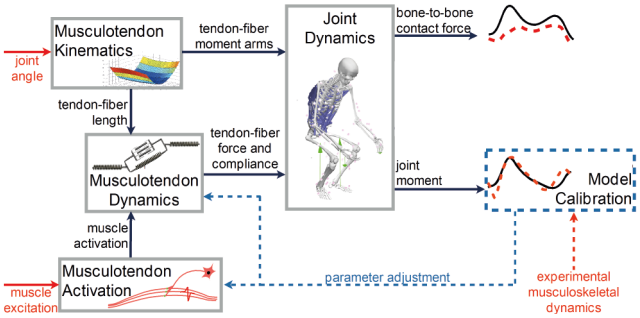

Fig. 1. CEINMS block diagram (adapted from [12]) constituted by five main blocks: MTU kinematics, MTU dynamics and MTU activation, joint dynamics and model calibration. The MTU kinematics block computes MTU lengths and moment arms from experimental joint angles. The MTU activation block maps the EMG activity to non-linear activations of model MTU. MTU forces are computed as a function of MTU activation and MTU kinematics in the MTU dynamics block. After calibration, the model operates in open-loop using EMG and joint kinematics as input.

C. Experimental protocol

1) Session I: After skin preparation and bipolar EMG electrode placement, maximum voluntary contractions trials (MVC) were recorded for all studied muscles. Then, reflective markers were placed as outlined in section II-A. The subject was asked to stand as still as possible and the static trial was recorded. Subsequently, the subject was instructed on how to perform the symmetrical lifting tasks. Two lifting techniques were used to symmetrically lift a box (22 x 40 x 30 cm) placed on the ground in front of the subject: squatting (SQ) and stooping (ST). Squatting consists of lifting the box while bending the knees and maintaining the trunk as upright as possible. Stooping involves lifting the box with extended knees. For each lifting technique, three different weight conditions were considered: no weight (0 kg), 5 and 15 kg. The subject had to complete a total of 36 lifting trials (6 trials per condition). Each trial consisted of 2 repetitions, and each repetition involved: (1) bending over to grab the box, (2) lifting the box until upright posture, (3) bending over to place the box and (4) returning to upright posture. After each trial, the subject rested for 1 minute to minimize muscle fatigue. The order in which the subject performed each of the 6 conditions was randomly pre-allocated to prevent potential order-related confounding effects.

2) Session II: After placing HDEMG grids as outlined in section II-A, MVC for lumbar and thoracic muscles was recorded. Then, reflective markers were placed and the static trial was recorded. Finally, the subject completed one lifting trial per condition: SQ (0 and 15 kg) and ST (0 and 15 kg). All tasks were performed similarly as in session I.

D. Data analysis

GRF, marker trajectories, bipolar EMG and monopolar HDEMG signals were processed using MOtoNMS Matlab toolbox [13]. GRF and marker trajectories were low-pass filtered (cut-off frequency: 6 Hz). Bipolar and HDEMG signals were processed to obtain EMG linear envelopes. Raw signals were: bandpass filtered (bandpass cut-off frequency: 30-300 Hz), full-wave rectified and low-pass filtered (cut-off frequency: 6 Hz). All filters were zero-lag 2^{nd} order Butterworth filters. MVC data from each specific experimental session were used to normalize the linear envelopes.

Following the data pre-processing, the LFB model was scaled using the 3D marker data from the static trials and the marker set described in section II-A. Then, marker trajectories from lifting trials were used to perform IK, thus, obtaining joint angles, MTU lengths and moment arms. For session I data, the weight of the box was added to the model as an external force. It was assumed that the weight of the box was equally distributed on both hands (2.5 kg on each hand for the 5 kg condition, and 7.5 kg for the 15 kg condition) and inertial properties of the box were neglected. Two vertical forces representing the weight were applied to the model's hands at the instant when the four bottom markers of the box experienced a vertical displacement of 1 cm. Finally, joint angles, GRF and box weight forces were used to obtain net joint moments via ID. Scaling, IK and ID were performed with OpenSim software [14].

TABLE I

MAPPING BETWEEN LFB MODEL MUSCLES AND MEASURED EMG CHANNELS. THE NUMBER OF MTUS WITHIN EACH MUSCLE GROUP IS INDICATED IN PARENTHESIS

LFB model muscle	EMG channel
Multifidus (50)	Longissimus pars lumborum
Longissimus thoracis pars lumborum (10)	Longissimus thoracis pars lumborum
Iliocostalis lumborum pars lumborum (8)	Iliocostalis pars lumborum
Longissimus thoracis pars thoracis (42)	Longissimus thoracis pars thoracis
Iliocostalis lumborum pars thoracis (16)	Longissimus thoracis pars thoracis
Psoas major (22)	Not assigned (passive)
Rectus abdominis (2)	Rectus abdominis
External oblique (12)	External oblique
Internal oblique (12)	Internal oblique
Quadratus lumborum (36)	Not assigned (passive)
Latissimus dorsi (28)	Not assigned (passive)

In order to drive the EMG-driven model (CEINMS), a mapping between the measured bipolar EMG channels and the LFB muscles was established (see Table I). Then, for each experimental condition, optimal fiber length, maximum isometric force and tendon slack length of the EMG-driven model MTUs were calibrated based on EMG signals, joint angles and ID moments (see Fig. 1). One individual lifting repetition was used to calibrate the model. The calibrated model was then used to compute the net L5/S1 flexion-extension (FE) moment and MTU forces for the remaining 11 repetitions, based exclusively on EMG and joint angles.

Root mean squared (RMS) values for normalized HDEMG linear envelopes were used to create topographical maps of muscle activation, during the lifts of session II. RMS values were computed using a 250 millisecond window.

III. RESULTS

The net FE moment at L5/S1 joint estimated via ID (reference moments) and CEINMS varied substantially throughout the lifting cycle (LC) (see Fig. 2, and Table II for a quantitative comparison of both estimates). Initially, during erect standing posture (0% LC), the ID moment for all conditions was approximately 0 Nm, meaning that the joint experienced either a slight extension or flexion moment. Here, during all SQ conditions and ST 0 kg condition, the CEINMS moment was approximately -40 Nm. Then, as the subject

TABLE II

ROOT MEAN SQUARED ERRORS (RMSE) AND R^2 BETWEEN ID AND CEINMS MOMENTS FOR ALL EXPERIMENTAL CONDITIONS

	Squat 0 kg	**Squat 5 kg**	**Squat 15 kg**	**Stoop 0 kg**	**Stoop 5 kg**	**Stoop 15 kg**
RMSE	11.31	10.73	14.09	10.23	11.70	20.30
$\mathbf{R^2}$	0.97	0.96	0.95	0.98	0.96	0.94

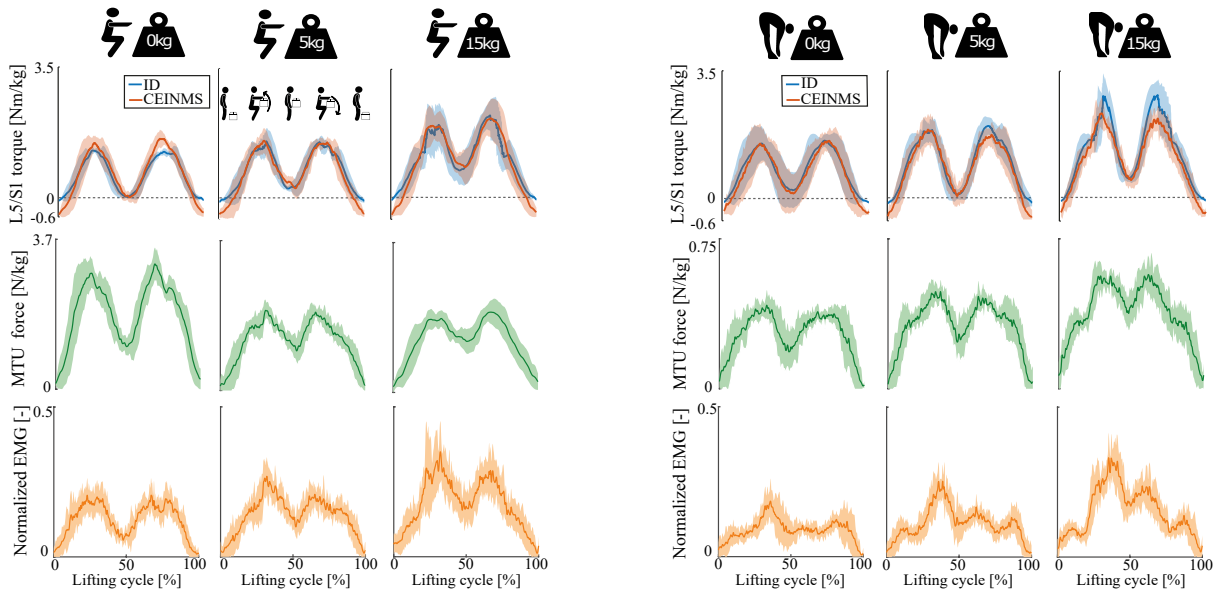

Fig. 2. L5/S1 flexion-extension moment estimated via ID and EMG-driven model (CEINMS), in blue and red respectively. CEINMS muscle forces (green) for a representative MTU of the longissimums thoracis pars lumborum muscle. Normalized EMG linear envelopes (orange) for longissimums thoracis pars lumborum muscle. Data are shown for the 6 experimental conditions of session I. Solid lines show the mean over all repetitions and the shaded areas correspond to $\pm$ 1 standard deviation. L5/S1 moments and MTU forces are normalized to body weight.

bent forward to grab the box the joint moment increased. Such increment was generally higher during stooping tasks (see Table III). During the 0 kg conditions, as soon as the subject lifted the box (25-30% LC), the FE moment started to decrease, until reaching 0 Nm (upright posture), for both ID and CEINMS. However, in the weight conditions, as soon as the subject lifted the box, the net moment experienced an increase due to its weight. For SQ with 5 and 15 kg, the increase was approximately 30 and 80 Nm, respectively. For ST with 5 and 15 kg, the increase was roughly 40 and 100 Nm, respectively. Moment changes in ID and CEINMS estimates were similar. Around 50% LC (standing while holding the weight), the moment was higher compared with the no weight conditions. For SQ 5 kg condition, the moment was approximately 20 Nm higher (SQ 15 kg, 50 Nm; ST 5 kg, 5 Nm; ST 15 kg, 40 Nm). At this point of the LC, similar moments were found for ID and CEINMS estimates. Thereupon, as the subject flexed to low down the box (65-75% LC), the moment progressively increased and finally, returned to initial standing levels when the trial finished.

TABLE III

MAXIMUM MEAN L5/S1 MOMENT ESTIMATED VIA ID AND CEINMS, MUSCLE FORCE AT REPRESENTATIVE MTU OF THE LONGISSIMUS THROACIS PARS LUMBORUM MUSCLE AND NORMALIZED EMG FOR ALL CONDITIONS. STANDARD DEVIATIONS ARE SHOWN IN PARENTHESIS

	CEINMS moment [Nm]	**ID moment [Nm]**	**MTU force [N]**	**EMG [-]**
Squat 0 kg	110.23 (16.80)	90.44 (10.53)	208.86 (27.07)	0.21 (0.05)
Squat 5 kg	106.75 (23.28)	105.70 (23.04)	133.59 (16.88)	0.27 (0.06)
Squat 15 kg	147.60 (34.49)	153.22 (28.70)	134.00 (19.42)	0.35 (0.07)
Stoop 0 kg	110.02 (22.13)	116.45 (12.73)	27.86 (5.01)	0.18 (0.07)
Stoop 5 kg	125.65 (28.34)	132.35 (16.06)	32.39 (3.64)	0.25 (0.05)
Stoop 15 kg	154.69 (24.36)	186.41 (40.93)	38.09 (6.12)	0.33 (0.08)

In a similar manner, EMG activity of all back muscles was substantially modulated across conditions. Fig. 2 and Table III report the measured EMG values of a representative muscle: the longissimus thoracis pars lumborum (LTL). During SQ conditions, the EMG signal of this muscle exhibited an analogous behavior as the joint moment: periods of increased activity (bending postures) and periods of low activity (upright postures). For ST lifting conditions, we observed a first peak of activity matching the box lifting but no similar peak while lowering it.

Muscle forces estimated via EMG-driven modeling experienced large differences across lifting techniques and weight conditions (Fig. 2 and Table III). The force generated by a specific MTU of the LTL muscle strongly decreased with increasing weight during SQ lifting. Nevertheless, during ST the force slightly increased with increasing weight and its magnitude was remarkably lower compared with SQ lifting.

Fig. 3 shows topographical maps created from HDEMG recordings, at specific stages of the LC for the 15 kg SQ condition. While the subject was standing upright, the overall activation of thoracolumbar musculature remained low (around 0.1). At the instant of lifting the box, EMG remarkably increased, being the center of activity located in more caudal regions. On the contrary, during the lowering movement, cranial regions of the back expressed a higher electrical activity.

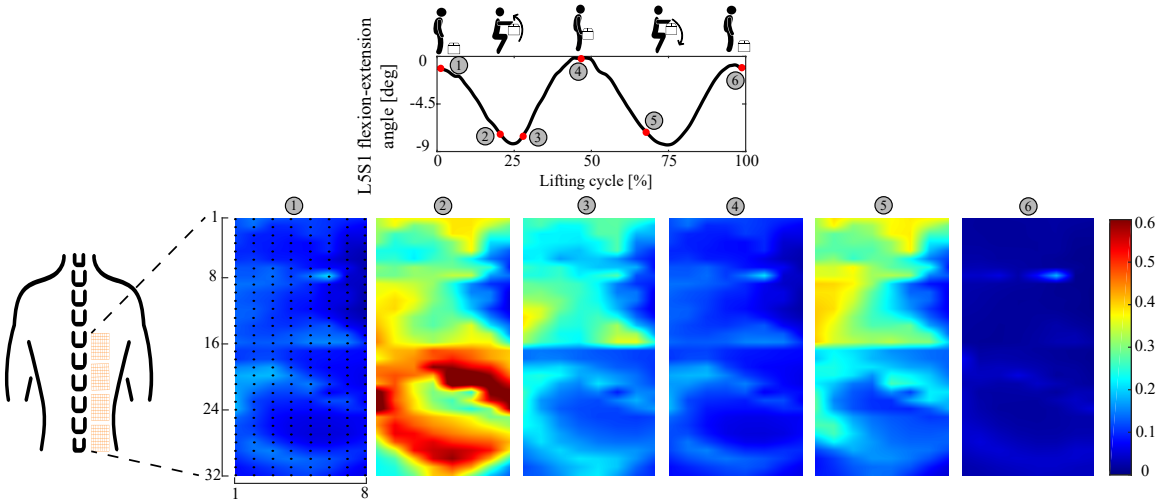

Fig. 3. Topographical maps (interpolated with 20-fold factor) of the normalized EMG RMS values obtained at 1%, 21%, 28%, 46%, 68% and 99% of the LC. The percentages correspond to: upright posture without box (start), lift-off of the box, beginning of box lifting, standing while holding the box, lowering down the box and upright posture without box (end), respectively. IK-derived L5/S1 FE angles are shown in the upper plot.

IV. DISCUSSION

The primary goal of the present study was to develop a framework which allows to measure high-resolution activation patterns of thoracolumbar muscles and to understand the relation between MTU forces and lumbar joint moments. As a first step, we validated an EMG-driven musculoskeletal modeling pipeline (based on our previously proposed CEINMS toolbox) to estimate moments around the lumbar joint L5/S1, during symmetric lifting tasks. We performed a quantitative comparison between CEINMS and the gold standard ID estimates. We found high correlation, R^2 (range: 0.94 - 0.98) and low RMSE (range: 10.23 - 20.30 Nm) values between ID and CEINMS estimates for the 6 experimental conditions. This suggested the validity of our EMG-driven model to accurately estimate the L5/S1 joint moment across a variety of lifting techniques and weight conditions.

For all SQ and ST 0 kg conditions, at the beginning and the end of the lifting trials we found a discrepancy of approximately 40 Nm of the CEINMS moment with respect to the ID gold standard. Such discrepancy may arise from inaccuracies in both, ID and CEINMS moment computations. During standing without holding weight, muscle activation is the lowest, therefore, passive tissue properties and musculoskeletal model geometry play a key role in moment estimation. More accurate ID estimates may be obtained by using imaging techniques to scale the LFB model. In the case of CEINMS, for each lifting and weight condition, we calibrated MTU parameters of our model (optimal fiber length, tendon-slack length and maximum isometric force) by using a specific lifting repetition. However, the calibration data only included the dynamic lifting movement and not a static standing posture component. Thus, we hypothesize that our model was not correctly calibrated for static postures. In future analyses, we will calibrate tendon-slack length and optimal fiber length, based on methods proposed in [15], which may improve the estimation of muscle passive forces.

We found the estimated ID and CEINMS overall moments to be higher during ST lifting compared with SQ for all weight conditions. These results agree with previous studies which compared the effects of lifting techniques on lumbar spine loading [16]. We also observed that lumbar moments generated during 15 kg weight conditions were substantially higher compared with 0 and 5 kg conditions. During 15 kg trials, peak moments were 35 - 45 Nm higher compared with 0 kg trials. Previous studies showed differences of approximately 20 Nm in L5/S1 peak moment, during symmetric lifting of 7 and 12 kg boxes [17]. This suggested that the sensitivity to differences in weight of our methodology is similar to that of previously validated approaches.

For both lifting techniques, increasing weights resulted not only in higher estimated moments (ID and CEINMS) but also, higher EMG activity (specifically, we show the longissimus thoracis pars lumborum muscle). Nevertheless, it is interesting to note that, in the case of MTU forces estimated via EMG-driven modeling, increasing weight did not always involve higher forces. For 15 kg SQ lifting, the muscle force generated at the representative MTU of the LTL muscle was roughly 70 N lower than for the no weight condition. In the case of ST lifting, the force generated when lifting 15 kg was approximately 10 N higher than with 0 kg. These preliminary results suggest a strong non-linearity between trunk muscle forces and joint moments, and highlight the need for a framework which provides a better understanding of trunk mechanics at a muscle level. In future studies, we will analyze the mechanisms underlying individual and collective MTU force generation.

Measured EMG revealed remarkable differences in muscle activation patterns across conditions. EMG activity was the highest during 15 kg lifting (SQ and ST) trials for all the measured muscles. Throughout the LC, it is possible to observe a double peak activation pattern in which, low activation periods reflect upright standing postures and high

activation ones, bent postures. The first activation peak matched the box lifting action (approx. 25% LC) while the second corresponded to the lowering of the box (approx 75% LC). It is possible to observe (Fig. 2) that for the weight conditions, the lift-off peak was higher than for the box-drop peak. This effect is more accentuated during ST conditions.

Topographical HDEMG maps obtained for the experimental session II, also contribute to understanding the different muscle recruitment strategies adopted by the subject across conditions. While most previous studies have focused on the lumbar regions of the erector spinae muscle [8], using 4 HDEMG grids (256 monopolar EMG channels) allowed us to analyze muscle activation in a much larger area, spanning lumbar and thoracic areas of the aforementioned muscle. In this paper, we showed changes in the topographical map for different stages of the lifting cycle for heavy weight (15 kg) SQ lifting. We observed that during weight lifting, the centroid of EMG activity was located in the caudal areas, that is, lumbar muscles. However, while lowering the weight, the centroid of HDEMG activity appeared in more cranial (thoracic) areas. This shift in muscle activation may explain the lower EMG activation peak observed in the LTL muscle while lowering of the box, during session I lifts. Similar motor unit recruitment or motor unit discharge rate adaptations have already been identified in other back muscles like the trapezius [18]. In these topographical maps, it is also possible to observe remarkable heterogeneity of activity across the entire examined region. These results are in line with previous studies which compared topographical maps for healthy and LBP subjects during lifting tasks [8].

A limitation of the present study is the reduced sample size. Only one healthy young subject was included, thus, results may not hold to groups such as older individuals. Furthermore, neglecting box inertial properties may introduce some error in torque estimates. However, we expect this to have a minor impact in the results due to slowness of lifting movements. Another limitation stems from the impossibility of validating muscle force estimates. In future studies, we will include a larger sample size and validate a single EMG-driven model, capable of estimating L5/S1 moments across a large repertoire of lifting conditions.

The ultimate goal of this research is the implementation of back-support exoskeleton control strategies based on real-time estimates of spinal compressive forces. In this study, we took the first step to validate our EMG-driven methodology to estimate such property. We showed valid estimates of FE L5/S1 moments, which are a basic component in the computation of compressive forces. In future studies, we will aim at validating the EMG-driven modeling approach to estimate compressive forces at the L5/S1 joint, offline and in real-time. Additionally, we showed the potential of our EMG-driven approach to analyze muscle force generation which, in contrast to other methodologies, allows us to understand muscle recruitment strategies. This, in combination with the potential of HDEMG recordings, constitutes a framework which will allow us to gain further understanding of the thoracolumbar neuromechanics during lifting tasks.

REFERENCES

[1] European Foundation for the Improvement of Living and Working Conditions., *5th European working conditions survey.* Publications Office of the European Union, 2012.

[2] P. Coenen, I. Kingma, C. R. L. Boot, J. W. R. Twisk, P. M. Bongers, and J. H. van Dieën, "Cumulative Low Back Load at Work as a Risk Factor of Low Back Pain: A Prospective Cohort Study," *Journal of Occupational Rehabilitation*, vol. 23, no. 1, pp. 11–18, mar 2013.

[3] G. Durandau, D. Farina, G. Asín-Prieto, I. Dimbwadyo-Terrer, S. Lerma-Lara, J. L. Pons, J. C. Moreno, and M. Sartori, "Voluntary control of wearable robotic exoskeletons by patients with paresis via neuromechanical modeling," *J NeuroEngineering Rehabil 16, 91*.

[4] H. Kazerooni, J.-L. Racine, Lihua Huang, and R. Steger, "On the Control of the Berkeley Lower Extremity Exoskeleton (BLEEX)," in *Proceedings of the 2005 IEEE International Conference on Robotics and Automation*. IEEE, pp. 4353–4360.

[5] M. P. De Looze, T. Bosch, F. Krause, K. S. Stadler, and L. W. O'sullivan, "Exoskeletons for industrial application and their potential effects on physical work load," *Ergonomics*, vol. 59, no. 5, pp. 671–681, 2016.

[6] H. Hara and Y. Sankai, "Development of HAL for lumbar support," *SCIS and ISIS 2010 - Joint 5th International Conference on Soft Computing and Intelligent Systems and 11th International Symposium on Advanced Intelligent Systems*, pp. 416–421, 2010.

[7] G. S. Faber, I. Kingma, A. J. Bakker, and J. H. van Dieën, "Low-back loading in lifting two loads beside the body compared to lifting one load in front of the body," *Journal of Biomechanics*, vol. 42, no. 1, pp. 35–41, jan 2009.

[8] D. Falla, L. Gizzi, M. Tschapek, J. Erlenwein, and F. Petzke, "Reduced task-induced variations in the distribution of activity across back muscle regions in individuals with low back pain," *Pain*, vol. 155, no. 5, pp. 944–953, 2014.

[9] E. Beaucage-Gauvreau, W. S. Robertson, S. C. Brandon, R. Fraser, B. J. Freeman, R. B. Graham, D. Thewlis, and C. F. Jones, "Validation of an OpenSim full-body model with detailed lumbar spine for estimating lower lumbar spine loads during symmetric and asymmetric lifting tasks," *Computer Methods in Biomechanics and Biomedical Engineering*, vol. 0, no. 0, pp. 1–14, 2019.

[10] I. Kingma, G. S. Faber, A. J. Bakker, and J. H. van Dieen, "Can Low Back Loading During Lifting Be Reduced by Placing One Leg Beside the Object to Be Lifted?" *Physical Therapy*, vol. 86, no. 8, pp. 1091–1105, 2006.

[11] C. Pizzolato, D. G. Lloyd, M. Sartori, E. Ceseracciu, T. F. Besier, B. J. Fregly, and M. Reggiani, "CEINMS: A toolbox to investigate the influence of different neural control solutions on the prediction of muscle excitation and joint moments during dynamic motor tasks," *Journal of Biomechanics*, 2015.

[12] M. Sartori, M. Reggiani, D. Farina, and D. G. Lloyd, "EMG-driven forward-dynamic estimation of muscle force and joint moment about multiple degrees of freedom in the huan lower extremity," *PLoS ONE*, vol. 7, no. 12, p. 52618, 2012.

[13] A. Mantoan, C. Pizzolato, M. Sartori, Z. Sawacha, C. Cobelli, and M. Reggiani, "MOtoNMS: A MATLAB toolbox to process motion data for neuromusculoskeletal modeling and simulation," *Source Code for Biology and Medicine*, vol. 10, p. 12, 2015.

[14] S. L. Delp, F. C. Anderson, A. S. Arnold, P. Loan, A. Habib, C. T. John, E. Guendelman, and D. G. Thelen, "OpenSim: Open-source software to create and analyze dynamic simulations of movement," *IEEE Transactions on Biomedical Engineering*, vol. 54, no. 11, pp. 1940–1950, nov 2007.

[15] C. R. Winby, D. G. Lloyd, and T. B. Kirk, "Evaluation of different analytical methods for subject-specific scaling of musculotendon parameters," *Journal of Biomechanics*, 2008.

[16] I. Kingma, G. S. Faber, and J. H. van Dieën, "Supporting the upper body with the hand on the thigh reduces back loading during lifting," *Journal of Biomechanics*, 2016.

[17] H.-K. Kim and Y. Zhang, "Estimation of lumbar spinal loading and trunk muscle forces during asymmetric lifting tasks: application of whole-body musculoskeletal modelling in OpenSim," *Ergonomics*, vol. 60, no. 4, pp. 563–576, 2017.

[18] D. Falla and D. Farina, "Non-uniform adaptation of motor unit discharge rates during sustained static contraction of the upper trapezius muscle," *Experimental Brain Research*, vol. 191, no. 3, pp. 363–370, 2008.